How to cite: *Angew. Chem. Int. Ed.* **2024**, *63*, e202316300
doi.org/10.1002/anie.202316300

Chiral TADF Emitters

Structural Control of Highly Efficient Thermally Activated Delayed Fluorescence in Carbene Zinc(II) Dithiolates**

Mousree Mitra[+], Ondřej Mrózek[+], Markus Putscher, Jasper Guhl, Benjamin Hupp, Andrey Belyaev, Christel M. Marian, and Andreas Steffen**

Abstract: Luminescent metal complexes based on earth abundant elements are a valuable target to substitute 4d/5d transition metal complexes as triplet emitters in advanced photonic applications. Whereas Cu^{I} complexes have been thoroughly investigated in the last two decades for this purpose, no structure-property-relationships for efficient luminescence involving triplet excited states from Zn^{II} complexes are established. Herein, we report on the design of monomeric carbene zinc(II) dithiolates (CZT) featuring a donor-acceptor-motif that leads to highly efficient thermally activated delayed fluorescence (TADF) with for Zn^{II} compounds unprecedented radiative rate constants $k_{TADF} = 1.2\times10^{6}\ s^{-1}$ at 297 K. Our high-level DFT/MRCI calculations revealed that the relative orientation of the ligands involved in the ligand-to-ligand charge transfer ($^{1/3}$LLCT) states is paramount to control the TADF process. Specifically, a dihedral angle of 36–40° leads to very efficient reverse intersystem-crossing (rISC) on the order of $10^{9}\ s^{-1}$ due to spin-orbit coupling (SOC) mediated by the sulfur atoms in combination with a small $\Delta E_{S1\text{-}T1}$ of ca. 56 meV.

Introduction

The investigation of 3d transition metal compounds as substitutes for precious metal complexes in photonic applications is a very timely topic.[1] One of the reasons is the comparably costly and energy-intensive production of 4d and 5d elements that are typically employed to facilitate and make use of photoinduced spin-forbidden processes due to their strong SOC, including phosphorescence as a radiative decay channel of triplet excited states. Another motivation is the search for new combinations of photophysical and photochemical properties and modes to control them. The last decade has seen a phoenix-like rise of the lighter and weaker SOC-mediating congeners of the d element complexes, with manifold applications of Zr^{IV},[2] $Cr^{0/III/VI}$,[3] Mn^{I},[4] $Fe^{II/III}$,[5] Co^{III},[6] Ni^{II}[7] and Cu^{I}[8] compounds in photo-induced energy (EnT) and electron transfer (ET), up-conversion, sensing, light-emitting devices, and as responsive smart materials. However, when it comes to efficient luminescence involving triplet excited states for device applications, copper(I) complexes in their d^{10} electron configuration are undoubtedly the prime choice among the 3d elements.[1a,8a–c,9] They do not feature detrimental metal-centered (MC) dd* states as potential non-radiative decay channels, and the weak SOC is sufficient for (r)ISC processes necessary for TADF, by which inefficient phosphorescence from the triplet excited states is bypassed and emission can occur from the singlet manifold. It is important to note the general photophysical differences between organic and transition metal TADF emitters. The latter usually exhibit a higher density of states (DOS) due to additional metal-to-ligand charge transfer (MLCT) or ligand-to-metal (LM)CT states promoting SOC, which influence the excited state kinetics. Consequently, the radiative lifetimes τ_{TADF} of organometallic TADF emitters at room temperature are typically shorter than observed for organics and can even surpass those of established Ir^{III} or Pt^{II} emitters.[8g,10] Although luminescent Cu^{I} complexes are well established, one of the limitations of their widespread usage is the high redox activity of the copper center, which can lead to premature degradation in electroluminescent devices.

An alternative that could resolve this issue are Zn^{II} complexes, where the metal ion features a considerably higher redox stability and a d^{10} electron configuration, hindering undesired non-radiative decay via MC states and allowing for modification of the coordination geometry to tune the photophysical properties. Only few Zn^{II} compounds with emission involving triplet excited states have been reported, most of which undergo facile non-radiative decay at room temperature and phosphoresce only at low

[*] M. Mitra,[+] Dr. O. Mrózek,[+] Dr. B. Hupp, Dr. A. Belyaev, Prof. Dr. A. Steffen
Faculty of Chemistry and Chemical Biology, TU Dortmund University
Otto-Hahn-Str. 6, 44227 Dortmund (Germany)
E-mail: andreas.steffen@tu-dortmund.de
M. Putscher, J. Guhl, Prof. Dr. C. M. Marian
Institute of Theoretical and Computational Chemistry, Faculty of Mathematics and Natural Sciences, Heinrich Heine University Düsseldorf
Universitätsstr. 1, 40225 Düsseldorf (Germany)
E-mail: Christel.Marian@hhu.de

[+] These authors contributed equally to this work.

[**] A previous version of this manuscript has been deposited on a preprint server (https://doi.org/10.26434/chemrxiv-2023-jt226).

temperatures.[11] Wenger and co-workers showed that the dark but long-lived ligand-centred (^{3}LC) states in zinc(II) complexes can be useful for application in photocatalysis, photoinduced ET and upconversion.[12] However, Bernhard and co-workers found indications that a hemi-cage analogue of fluorescent $[Zn(bpy)_3]^{2+}$ bearing a hexadentate bipyridyl-based ligand shows phosphorescence from a ^{3}LC state with $\tau = 70$ ns in solution at room temperature, albeit with low quantum yields of $\Phi = 0.07$.[11g] Heteroleptic zinc(II) 1,10-phenanthroline bis(thiophenolates) exhibit excited states of LLCT character and have been studied in detail by Crosby et al.[11h,i] Although the emission is very weak at room temperature, very recently we were able to show that the dominant radiative path is TADF.[13] Adachi and co-workers found in $[Zn(PX\text{-}BOX\text{-}O)_2]$ (PX-BOX-O=bis(2-(benzo[d]oxazol-2-yl)-5-(10H-phenoxazin-10-yl)phenolate) a delayed component with $\Phi_{TADF} = 0.48$–0.66 beside prompt fluorescence ($\Phi_{Fl} = 0.10$–0.12) from intra-ligand ($^{1/3}$IL)CT states. The rISC is moderately efficient with $k_{rISC} = 1.4$–$16.9\times10^4\ s^{-1}$, but proof-of-concept application in OLEDs demonstrates the potential of Zn^{II} complexes.[11j]

In contrast to Cu^I complexes featuring MLCT states that can mediate SOC for spin-forbidden processes, the d orbitals of the Zn^{II} ion do not participate in the excited states in the above-mentioned examples, which explains the low to moderate triplet emission performance. In order to improve the TADF process by enhancing the DOS,[14] we have started to develop a fundamentally different class of Zn^{II} emitters bearing cyclic(alkyl)(amino) carbenes (cAAC) as potent excited-state π-acceptors, which can provide access to LLCT states with an admixture of unusual LMCT.[15] Following our initial report on phosphorescent $[ZnX_2(^{Me}cAAC)_2]_2$ with ultra-long lifetimes,[15a] we developed the first dimeric carbene-zinc-thiolate (CZT) $[Zn(bdt)(^{Me}cAAC)]_2$ (bdt = benzene-1,2-dithiolate) with a suitable donor-acceptor motif for this purpose (Scheme 1).[15b]

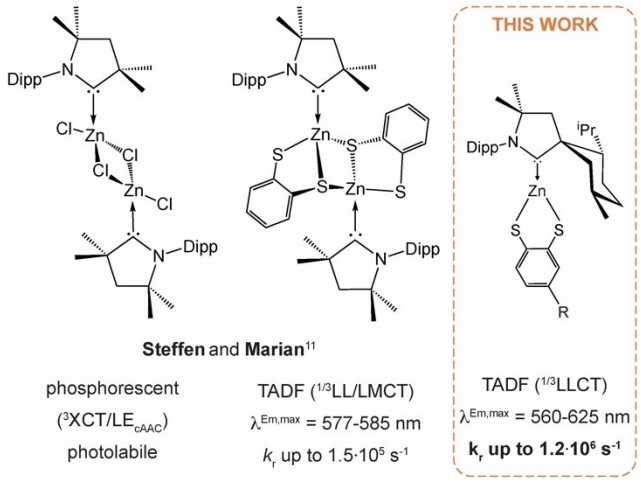

Scheme 1. Development of luminescent Zn^{II} carbene complexes. Left: phosphorescent Zn^{II} halide carbenes. Middle: first example of a carbene-zinc-thiolate (CZT) showing TADF. Right: latest generation of CZT-TADF emitters.

Indeed, the resulting small energy gap $\Delta E_{S1\text{-}T1}$ of 79 meV allows for efficient rISC and TADF with good k_{TADF} of up to $1.5\times10^5\ s^{-1}$ in dichloromethane solution at room temperature. Although these results clearly demonstrate the potential of our approach, and the compound is even stable in oxygen-saturated wet organic solvents under UV irradiation, the main drawback remains the moderate $\Phi = 0.1$ in PMMA matrix.[15b] Herein, we report on a new generation of monomeric CZT complexes composed of sterically demanding menthyl-substituted cAAC (^{Menth}cAAC) and various bdt derivatives, giving highly efficient TADF for Zn^{II} complexes with unprecedented k_{TADF} of up to $1.2\times10^6\ s^{-1}$ at 297 K.

Results and Discussion

The target compounds $[Zn(^{R}bdt)(^{Menth}cAAC)]$ (R = 4-H (**CZT1**), 4-Me (**CZT2**), 4-^{t}Bu (**CZT3**)) were prepared by a two-step protocol (Scheme 2, top), starting with addition of ^{Menth}cAAC to $ZnCl_2$ to afford the synthon $[ZnCl_2(^{Menth}cAAC)]$ (**1**). We found **1** to be highly reactive and unstable, leading to contamination with protonated carbene independent of the purification methods. Although this prevented its full characterization, single crystals were obtained by gas phase diffusion of *n*-pentane into a THF solution of **1** (Figure S9). However, in situ generation of **1** and subsequent halide exchange with the disodium salt of the respective 4-R-benzene-1,2-dithiolate provides facile access to monomeric **CZT1–3**. The compounds are highly soluble and stable in THF, dichloromethane and toluene, which we attribute to the chelating coordination of the bdt

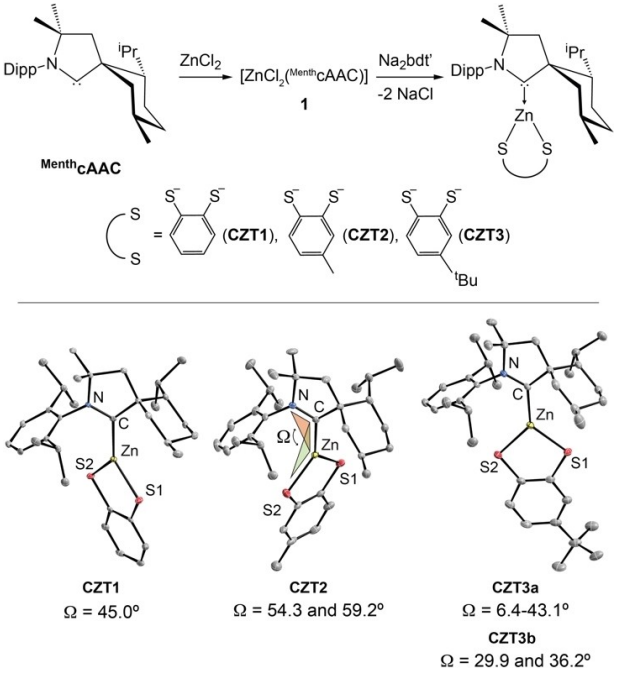

Scheme 2. Top: Synthesis of **1** and **CZT1–3**. Bottom: Molecular structures of **CZT1–3** and their dihedral angles Ω. Hydrogen atoms are omitted for clarity.

ligands and the steric protection of the Zn–C(cAAC) bond. Remarkably, the ^{t}Bu moiety in **CZT3** not only leads to additional solubility in *n*-pentane, but greatly enhances the stability in solution even in the presence of water (Figure S7).

The $^{13}C\{^{1}H\}$ NMR resonance of the carbene carbon in **CZT1–3** at ≈245 ppm shows a significant upfield shift in comparison to the free ligand (319 ppm)[16] and thus clearly proves successful coordination of ^{Menth}cAAC to the Zn^{II} ion. In addition, the ^{1}H and ^{13}C NMR spectroscopic measurements of **CZT1–3** also show only one set of sharp signals, arguing for barrier-free rotation of the carbene and/or dithiolate ligands at room temperature. Indeed, our DFT calculations confirm a very low rotational energy barrier of only 4 kJ/mol for **CZT1** (Figure S16). Single crystal X-ray diffraction studies reveal a trigonal planar coordination of the zinc(II) center in **1** and **CZT1–3** (Scheme 2, bottom).[17] For all complexes the Zn–$C^{CARBENE}$ interatomic distances have comparable values in the range of 2.015–2.045 pm. The Zn–Cl and Zn–S distances of ≈2.2 pm found in **1**, and **CZT1**/**CZT2**, respectively, are in the range typically found for related Zn^{II} halide and aromatic dithiolate complexes.[15b,18] The molecular packing in the solid state is influenced by the bdt substituents in the 4-position, leading to different dihedral angles Ω between the S–Zn–S plane and the carbene plane of 45° and 59° for **CZT1** and **CZT2**, respectively. Interestingly, we were able to isolate different ligand conformations upon recrystallization of **CZT3** from either THF/*n*-pentane (**CZT3a**) or toluene/cyclohexane (**CZT3b**) mixtures (Scheme 2), which greatly affect the excited state behavior (see below). In the case of **CZT3a**, the unit cell comprises eight independent molecules with values of Ω between 6.4–43.1°, whereas for **CZT3b** only two independent molecules with Ω of 29.9 and 36.2° were found (Table S1).

The electronic UV/Vis absorption spectra of **CZT1–3** in dichloromethane show a very broad low intensity band between 350–480 nm that we assign to a π(bdt)→π*(C–N, cAAC) transition of LLCT character according to our DFT/MRCI studies, which is sensitive to the dihedral angle Ω between the ligands (Figure 1). A tilted conformation (calc. $\Omega_{S0}=40°$) is the most stable one in the electronic ground state, and a scan of the torsional potential shows that nearly planar ($\Omega_{S0}=10°$) and orthogonal ($\Omega_{S0}=76°$) conformers are separated by only small energy barriers, which are easily surmounted at ambient temperatures (Figure S16).

Consequently, the extinction coefficients $\varepsilon=3{,}500$–$3{,}800\ M^{-1}cm^{-1}$ represent averages over all conformers in solution due to the high fluxionality of the complexes. Substitution of the bdt ligand in the 4-position in **CZT2** and **CZT3** gives rise to only a very minor bathochromic shift of this band. The more intense ($\varepsilon \approx 8{,}900$–$9{,}300\ M^{-1}cm^{-1}$) band between 290–330 nm shows two maxima and originates from an LLCT transition related to an excitation from the sulfur lone pairs (n) to the C–N π* orbital of the cAAC, and an LC ππ*(bdt) state (see also Tables S9–S11). The high energy region (below 280 nm) is dominated by allowed, high intensity bands of ^{1}LC (ππ*) character.

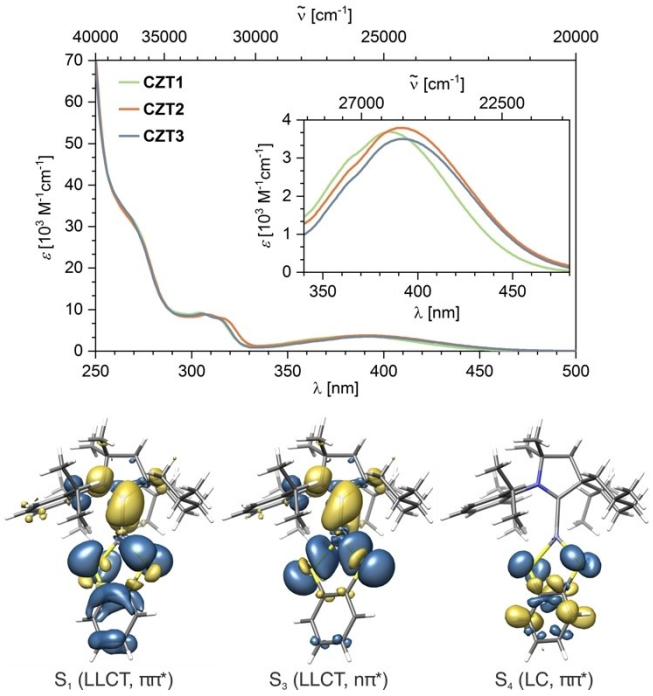

Figure 1. Experimental UV/Vis absorption spectra of **CZT1–3** in CH_2Cl_2 solution at room temperature and electron density differences of the transitions from the ground state S_0 to the S_1 (^{1}LLCT, ππ*), S_3 (^{1}LLCT, nπ*) and S_4 (^{1}LC, ππ*) excited states (calculated at the DFT/MRCI level of theory; loss of electron density is indicated in blue and gain in yellow; isosurface values ±0.002; see also ESI).

Upon irradiation of powder samples of **CZT1–3** with $\lambda_{ex}<450$ nm, bright yellow-to-orange photoluminescence with large Stokes shift ($\lambda_{max}=560$–583 nm) apparently from an LLCT state is observed at room temperature (Figure 2, Table 1). In comparison to previously reported dimeric $[Zn(bdt)(^{Me}cAAC)]_2$, which displays a small photoluminescence quantum yield $\Phi=0.02$,[15b] the efficiency of the monomers is 6–15 times enhanced to reach values of up to 0.29 for **CZT3**. The observed averaged luminescence lifetimes of $\tau_{av}=170$–630 ns suggest radiative rate constants of $k_r=4.5$ (**CZT1**), 7.5 (**CZT2**) and 7.4×10^{5} (**CZT3**) s^{-1}, that are higher by more than one order of magnitude than found for the dimer[15b] and indicative of triplet excited states being involved. Although the luminescence quantum yields are decreased in PMMA or polystyrene films for **CZT2** and **CZT3**, the k_r are still in the range of $10^{5}\ s^{-1}$ (Table 1). The broad LLCT emission is also observed in CH_2Cl_2 solution at room temperature (Figure S11), but the high fluxionality of the complexes in solution (see above) leads to very facile non-radiative decay and prevents further analysis.

Bearing in mind that Zn^{II} does not mediate strong SOC for fast phosphorescence,[13,15] we were curious whether the zinc dithiolate complexes emit via TADF and thus we carried out time-resolved variable temperature (tr-VT) luminescence studies. Indeed, the luminescence lifetimes τ_{av} of **CZT1–3** in the solid state increase by several orders of magnitude at 77 K, where we were able to experimentally determine Φ_{77K}, giving rise to much smaller $k_r=2.5\times10^{2}$–

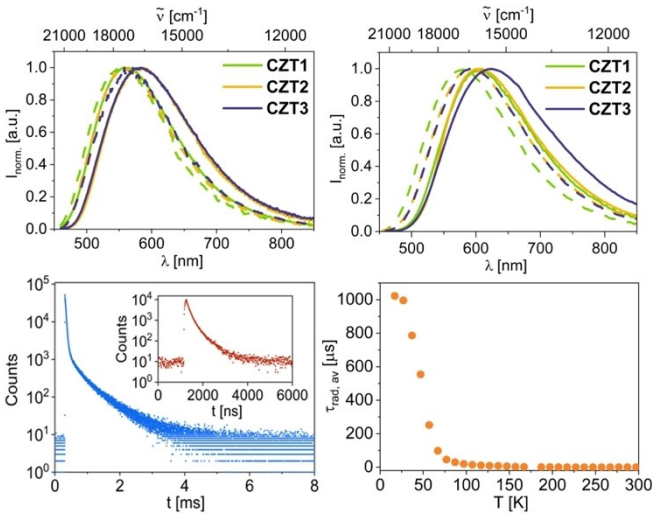

Figure 2. Top left: Photoluminescence of **CZT1–3** in the solid state at room temperature (dashed lines) and at 77 K (solid lines). Top right: Photoluminescence of **CZT1–3** in 1 wt% PS (solid lines) and PMMA (dashed lines). Bottom left: Photoluminescence decay of **CZT2** at 77 K and 297 K (inset) in the solid state. Bottom right: temperature-dependence of the averaged radiative lifetimes $\tau_{av,rad}$ of **CZT2**.

6.7×10^3 s^{-1} (Table 1). Upon further cooling compound **CZT2** to <50 K, a luminescence lifetime plateau is observed in the millisecond regime (Figure 2, and Table S7).

Such a photophysical behavior is typical for a temperature-dependent Boltzmann equilibrium between states of very different oscillator strength and cannot be explained by regular phosphorescence, but rather by TADF involving states of different spin multiplicity.

Noteworthy, the transient luminescence decays are biexponential at 297 K, but at lower temperatures become multiexponential with 3–4 lifetime components (Figure 2). Presumably this is due to the structural flexibility of the Zn^{II} complexes, i.e., several conformers with different dihedral angles Ω between the ligands being present in the powder samples, which give rise to different emitting excited state geometries with different Franck–Condon factors. Indeed, upon isolating larger amounts of polymorph **CTZ3a** containing eight independent molecules with different Ω we observed very complex transient luminescence decays of the single crystals. Under such conditions, k_r obtained from the average lifetime τ_{av} is not an appropriate descriptor for an in-depth analysis because the observed luminescence properties are not related to a single species or may be due to different excited state geometries. However, the modelling of the kinetic processes for population of the emitting excited states involved in the TADF process assumes a three-state-scenario between S_0, S_1 and T_1, with each of them exhibiting only one geometry that is dominantly responsible for the respective transition.

We were able to isolate larger quantities of single-crystalline material of polymorph **CZT3b** that contains two independent molecules in the unit cell with very similar dihedrals Ω of 29.9° and 36.2°, respectively, and which exhibits only biexponential lifetime decays, allowing for a more detailed analysis. Both decay channels contribute to the TADF process as indicated by their VT behavior in Figure 3. At 27 K, we observed long lifetimes of 2.9 and 7.7 ms, which suggests that the involved triplet excited states experience very weak SOC and that they differ in their geometry or character. Upon increasing the temperature, the excited states responsible for the two emission paths interconvert as the relative contributions of τ_1 and τ_2 change (see below). Between 257–297 K, they appear to be in thermal equilibrium (see Table S8) because the contributions remain constant and thus τ_{av} is an appropriate approximation to evaluate k_r of **CTZ3b**, giving a record value for Zn^{II}-based emitters of 1.2×10^6 s^{-1} and high $\Phi=0.49$ at room temperature (Table 1).

Fitting the VT lifetime data of either the single lifetime components of **CZT3b** or their average according to eq. 1 in the temperature range between 27–297 K using an established three-state kinetic model provides deeper insight into the TADF parameters. The obtained energy gap $\Delta E_{S1\text{-}T1}$ appears to be as low as 56 meV (452 cm^{-1}), which is sufficiently small to allow for efficient rISC $T_1\rightarrow S_1$, and in

Table 1: Photophysical data of **CTZ1–3** in the solid state and doped in polymer matrices (1 wt-%).

	medium	T / K	λ_{max} / nm	[a] τ_{av} / µs	Φ	[b] k_r / s^{-1}		medium	T / K	λ_{max} / nm	[a] τ_{av} / µs	Φ	[b] k_r / s^{-1}
CZT1	Powder	297	560	0.63	0.28	4.5×10^5	**CZT3**	Powder	297	580	0.45	0.33	7.3×10^5
		77	556	1940	0.49	2.5×10^2			77	570	1149	0.76	6.6×10^2
	PMMA	297	570	0.28	0.02	7.2×10^4		PMMA	297	592	0.30	0.16	5.3×10^5
	PS	297	605	0.19	0.01	5.2×10^4		PS	297	625	0.21	0.12	5.7×10^5
CZT2	Powder	297	583	0.17	0.13	7.5×10^5	**CTZ3a**	Crystals	297	577	0.95	0.29	3.1×10^5
		77	568	46	0.31	6.7×10^3		(Ω = 6-43°)	77	561	1220	0.48	3.9×10^2
	PMMA	297	590	0.22	0.06	2.7×10^5	**CTZ3b**	Crystals	297	580	0.39	0.49	1.2×10^6
	PS	297	607	0.21	0.03	1.4×10^5		(Ω = 30/36°)	77	553	346	0.97	2.8×10^3

[a] For multiexponential decays, the amplitude averaged lifetimes are given (see also Supporting Information). [b] $k_r=\Phi/\tau$.

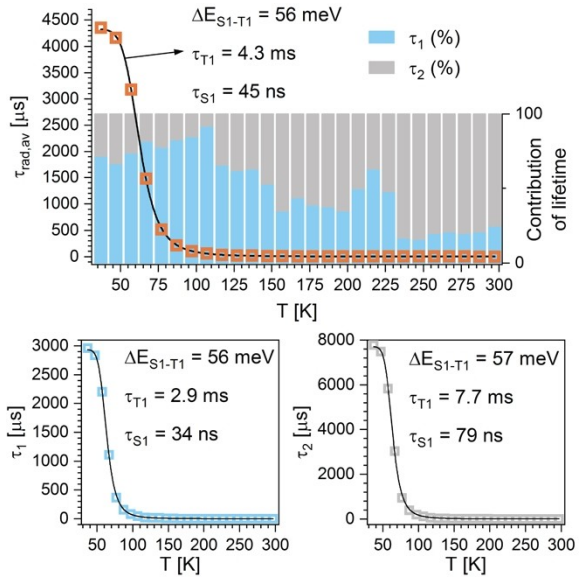

Figure 3. Top: Temperature-dependence of the averaged radiative lifetime $\tau_{rad,av}$ of **CZT3b** and relative contributions of τ_1 and τ_2. Bottom: Temperature-dependence of τ_1 and τ_2. The black lines represent the fit of the experimental data according to eq 1, and the obtained fitting parameters of the TADF are given in the graphs.

combination with a short τ_{S1} = 34–79 ns (k_F = 1.2–2.9×10^7 s^{-1}) for fast TADF (Figure 3).

$$\frac{1}{k_r} = \tau_{rad} = \frac{3 + \exp\left[-\frac{\Delta E^{S1-T1}}{k_B T}\right]}{3k_P + k_F \cdot \exp\left[-\frac{\Delta E^{S1-T1}}{k_B T}\right]} \quad (1)$$

As mentioned above, our DFT/MRCI calculations of the model compound **CZT1** show that tilted, near-planar and orthogonal conformations of the ligands are very close in energy in the electronic ground state S_0. A similar situation is found for the singlet and triplet excited states S_1 and T_1, which are responsible for the TADF mechanism. On the ^{1}LLCT(ππ*) potential energy surface, a slight preference for the planar conformer is observed, with the tilted (ΔE_{S1} = 160 cm^{-1}) and orthogonal (ΔE_{S1} = 260 cm^{-1}) being marginally higher in energy. Despite their small energy differences,

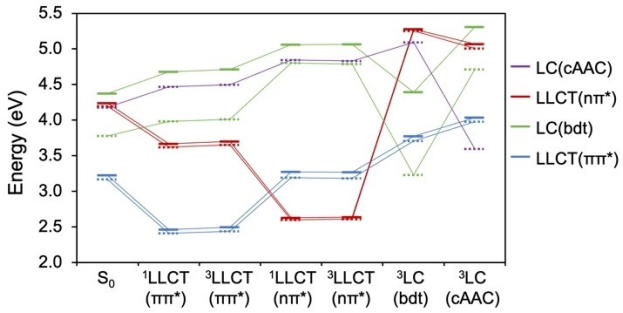

Figure 4. DFT/MRCI excitation energies of the relevant states at different geometries for model compound **CZT1** (tilted conformer). All energies are calculated relative to the ground state energy at the S_0 geometry.

the minima exhibit considerably different photophysical properties and thus may explain the observed multiexponential lifetime decays as well as the different T_1 lifetimes at very low temperatures (Table 2). The variation of the fluorescence rate constant follows the expectation that the oscillator strength of a ^{1}LLCT(ππ*) transition is highest for a coplanar orientation of the donor and acceptor moieties, giving k_F = 1.0×10^7 s^{-1}. Even the increase of the phosphorescence rates with increasing twist angle can be explained by a simple model based on El-Sayed's rules. Because SOC preferentially couples ^{3}ππ* states with ^{1}nπ* states, the ^{3}LLCT(ππ*) phosphorescence primarily borrows intensity from an energetically higher lying, spin-allowed ^{1}LLCT (nπ*)→S_0 transition (Figure 4 and Tables S10–S13), which is strongest for the orthogonal conformer and leads to k_P = 939 s^{-1} (Table 2). Here, the highest occupied nonbonding sulfur n MO and the C–N antibonding π* MO of the carbene exhibit similar symmetry properties (Figure S17), thus facilitating the electric dipole transition.

Highly important for the TADF efficiency and evaluation of structure–property relationships is the finding that ISC and rISC become ultrafast in the tilted conformation of the S_1 and T_1 states (Table 2). At 298 K, these formally spin-forbidden processes occur with calculated rate constants of k_{ISC} = 3×10^{10} and k_{rISC} = 5×10^9 s^{-1} due to the unusually large mutual $^{1/3}$LLCT(ππ*) SOC in combination with a small energy gap ΔE_{S1-T1} of only 153 cm^{-1}. Typically, singlet and

Table 2: DFT/MRCI calculated parameters of the model complex **CZT1** relevant for the TADF process of this general class of emitters.

Conformer	Dihedral angle Ω[a]	ΔE(S$_1$–T$_1$)[b] / cm^{-1}	Σ SOCME^2 / cm^{-2}		k_{ISC}[c] / s^{-1}		k_{rISC}[c] / s^{-1}		k_F / s^{-1}	k_P / s^{-1}	k_{TADF}[d] / s^{-1}
			S$_1$	T$_1$	298 K	77 K	298 K	77 K			
Planar	10/17/13°	195/281	3.1	1.8	2×10^9	1×10^9	6×10^7	9×10^5	1.0×10^7	2	3.3×10^5
Tilted	40/38/36°	223/153	21.6	20.1	3×10^{10}	3×10^{10}	5×10^9	7×10^8	7.8×10^6	31	1.2×10^6
Ortho	76/76/80°	157/594	8.9	7.2	5×10^9	6×10^9	9×10^6	1×10^4	1.3×10^6	939	3.5×10^3
Kinked	–/29/31°	133/155	2.2	3.4	2×10^9	4×10^8	4×10^8	1×10^7	7.4×10^4	1570	3.5×10^3

[a] For the definition of Ω, see Scheme 2. Values are displayed for S_0/S_1/T_1. [b] Adiabatic energy gap excluding/including zero-point vibrational energy corrections. [c] k_{ISC} and k_{rISC} have been calculated independently. [d] $k_{TADF} = k_F$ (k_{rISC}/k_{ISC})

triplet states with similar electronic structures exhibit tiny SOC matrix elements. However, the bdt ligand in the tilted conformer is slightly kinked at the sulfur atoms, which leads to a small admixture of LLCT(nπ*) character into the LLCT(ππ*) wavefunction, sufficient to increase the SOC because the π and n orbitals both exhibit large amplitudes at the sulfur centers (Figure S18). In addition, the relative excited state kinetics k_{ISC}/k_{rISC} provide the most favorable steady-state equilibrium $T_1 \leftrightarrow S_1$ for the tilted conformation with Ω values as observed for polymorph **CZT3b**, giving a theoretically calculated rate constant for delayed fluorescence of $k_{TADF} = 1.2\times10^6\ s^{-1}$ at 298 K (Table 2). This is fully consistent with the obtained experimental value and thus provides a structural design criterium for exceptionally fast TADF in Zn^{II} complexes.

Although the global minima of the S_1 and T_1 states are of $^{1/3}$LLCT(ππ*) character, local minima arise from the $^{1/3}$LLCT(nπ*) excitation with a conformation, which does not have a counterpart in the electronic ground state (Figure 4 and Table S13). Characteristic of the nuclear arrangements are bdt kink angles (S–Zn–S–C) close to 50°, which are unfavorable for the LLCT(ππ*) electronic structure, resulting in a conical intersection of their potential energy surfaces (Figure 5).

Adiabatically, the $^{1/3}$LLCT(nπ*) minima are located ca. 1500 cm^{-1} above the planar $^{1/3}$LLCT(ππ*) structures. Due to the large geometry displacements between the initial and final states, (r)ISC rate constants cannot be determined with high confidence. However, based on values of $\approx10^4\ cm^{-2}$ for the component-averaged squared $^{1/3}$LLCT(nπ*)-$^{3/1}$LLCT(ππ*) SOC, downhill ISC processes are estimated to proceed on the (sub)nanosecond timescale, despite the moderate vibrational overlap. Uphill $^{3/1}$LLCT(ππ*)-$^{1/3}$LLCT(nπ*) transitions are not expected to occur. Considering the comparably low k_F (Table 2), ^{1}LLCT(nπ*) fluorescence cannot compete against nonradiative deactivation. Noteworthy, the weaker SOC and smaller k_{rISC} of the non-tilted conformations results in diminished calculated k_{TADF} values of 3.5×10^3–$3.5\times10^5\ s^{-1}$, which explains the different experimental radiative rate constants found in dependence of the aggregation state or medium at room temperature in these geometrically fluxional emitters (Table 1).

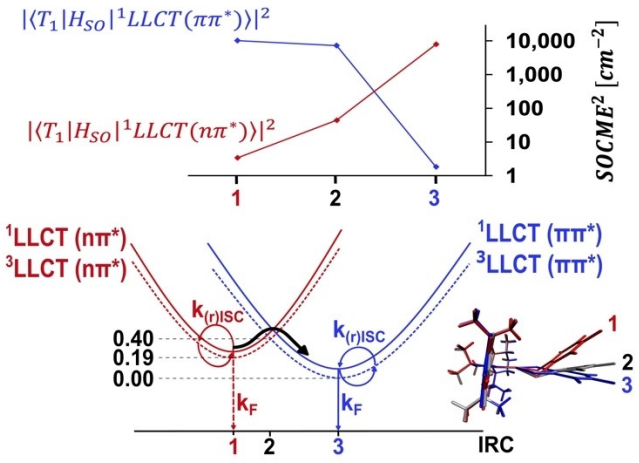

Figure 5. Bottom left: Schematic energy profiles of the ^{1}LLCT (solid lines) and ^{3}LLCT states (dashed lines) of **CZT1** along an intrinsic reaction coordinate (IRC) connecting the minima of the ^{3}LLCT(nπ*) (**1**) and ^{3}LLCT(ππ*) (**3**) states. The crossing point (**2**) of the ^{3}LLCT(nπ*) and ^{3}LLCT(ππ*) potential energy surfaces is located energetically 0.21 eV above the ^{3}LLCT(nπ*) minimum and 0.40 eV above the ^{3}LLCT(ππ*) minimum at the DFT/MRCI level of theory. Molecules populating initially the LLCT(nπ*) states decay preferentially to the LLCT(ππ*) state which emit prompt and delayed fluorescence. Bottom right: Nuclear arrangements of **CTZ1** at the geometry points **1**–**3**. The bdt ligand is strongly kinked in the ^{3}LLCT(nπ*) state whereas the benzene and S–Zn–S plane exhibit an angle close to 180° in the ^{3}LLCT(ππ*) state. Top: Spin-orbit strength of the T_1 state at the geometry points **1**–**3**. T_1 exhibits ^{3}LLCT(nπ*) at points **1** and **2** and ^{3}LLCT(ππ*) character at point **3**.

Conclusion

The monomeric Zn^{II} TADF emitters **CZT1**–**3** reported herein exhibit greatly increased k_r by up to one order of magnitude and 25-fold enhancement of φ in comparison to previously reported dimeric $[Zn(bdt)(^{Me}cAAC)]_2$, although the electronic properties of the ^{Menth}cAAC ligand generally resemble those of the less bulky derivate ^{Me}cAAC. Time-resolved variable temperature luminescence studies on polymorphs of $[Zn(bdt^{tBu})(^{Menth}cAAC)]$ (**CZT3**) in conjunction with high-level DFT/MRCI calculations revealed that the relative orientation of the ligands involved in the $^{1/3}$LLCT states is paramount to control the TADF properties. The inefficient TADF dimers $[Zn(bdt)(^{Me}cAAC)]_2$ feature bdt ligands lying entirely out of the plane of the carbene ligand (Scheme 1). In contrast, the dihedral angle of 33–36° in **CZT3b** leads to very efficient rISC on the order of $10^9\ s^{-1}$ due to SOC mediated by the sulfur atoms in combination with a small $\Delta E_{S1\text{-}T1}$ of ca. 56 meV. Consequently, a high $k_{TADF} = 1.2\times10^6\ s^{-1}$ is obtained at room temperature, which is exceptional for Zn^{II} based emitters involving triplet excited states.

A comparison with other Zn^{II} complexes emitting via TADF is imperative and highlights our design strategy using $^{1/3}$LLCT states that can be sterically controlled for achieving high k_r. Adachi and co-workers demonstrated that Zn^{II} complexes emitting via TADF from $^{1/3}$ILCT states can achieve k_{TADF} of ca. $2\times10^4\ s^{-1}$.[11j] Luminescent Schiff-base Zn^{II} complexes have also been reported to show TADF from an equilibrium of $^{1/3}$ILCT states, albeit with low quantum yields as the major decay path is prompt fluorescence and ISC/rISC processes are inefficient.[19] Clearly, the construction of nearly degenerate $^{1/3}$LLCT/LMCT states with SOC contribution from the heteroatoms of the ligands is superior and leads to the fastest Zn^{II} based triplet emitters to date, of which the k_{TADF} of up to $1.2\times10^6\ s^{-1}$ are even competitive to well-established triplet emitters applied in commercial devices based on rare 4d/5d transition metals.

Supporting Information

The authors have cited additional references within the Supporting Information.[20–46]

Acknowledgements

This work was supported by Deutsche Forschungsgemeinschaft [DFG, Priority Program SPP 2102 "Light-controlled reactivity of metal complexes" (MA 1051/18-1 and STE 1834/7-1)]. We are also grateful to the DFG for funding of major research equipment (INST 212/430-1 FUGG and INST 212/455-1 FUGG). A.B. is grateful to Alexander von Humboldt Foundation for a Research Fellowship grant for Postdoctoral Research. We thank Prof. M. Hansmann (TU Dortmund University) for providing a sample of racemic carbene ligand for initial experiments. Open Access funding enabled and organized by Projekt DEAL.

Conflict of Interest

The authors declare no conflict of interest.

Data Availability Statement

The data that support the findings of this study are available in the supplementary material of this article.

Keywords: Carbenes · Circularly Polarized Luminescence · DFT/MRCI · TADF · Zinc

[1] a) A. Steffen, B. Hupp, in *Comprehensive Coordination Chemistry III* (Eds.: E. C. Constable, G. Parkin, L. Que, Jr.), Elsevier, Oxford, **2021**, pp. 466–502; b) O. S. Wenger, *J. Am. Chem. Soc.* **2018**, *140*, 13522–13533; c) C. Förster, K. Heinze, *Chem. Soc. Rev.* **2020**, *49*, 1057–1070; d) C. Wegeberg, O. S. Wenger, *JACS Au* **2021**, *1*, 1860–1876; e) N. Sinha, O. S. Wenger, *J. Am. Chem. Soc.* **2023**, *145*, 4903–4920.

[2] a) Y. Zhang, T. S. Lee, J. L. Petersen, C. Milsmann, *J. Am. Chem. Soc.* **2018**, *140*, 5934–5947; b) Y. Zhang, T. S. Lee, J. M. Favale, D. C. Leary, J. L. Petersen, G. D. Scholes, F. N. Castellano, C. Milsmann, *Nat. Chem.* **2020**, *12*, 345–352; c) M. Yang, S. Sheykhi, Y. Zhang, C. Milsmann, F. N. Castellano, *Chem. Sci.* **2021**, *12*, 9069–9077.

[3] a) C. Wang, F. Reichenauer, W. R. Kitzmann, C. Kerzig, K. Heinze, U. Resch-Genger, *Angew. Chem. Int. Ed.* **2022**, *61*, e202202238; b) N. Sinha, C. Wegeberg, D. Häussinger, A. Prescimone, O. S. Wenger, *Nat. Chem.* **2023**, *15*, 1730–736; c) T. H. Bürgin, F. Glaser, O. S. Wenger, *J. Am. Chem. Soc.* **2022**, *144*, 14181–14194; d) F. Reichenauer, C. Wang, C. Förster, P. Boden, N. Ugur, R. Báez-Cruz, J. Kalmbach, L. M. Carrella, E. Rentschler, C. Ramanan, G. Niedner-Schatteburg, M. Gerhards, M. Seitz, U. Resch-Genger, K. Heinze, *J. Am. Chem. Soc.* **2021**, *143*, 11843–11855.

[4] P. Herr, C. Kerzig, C. B. Larsen, D. Häussinger, O. S. Wenger, *Nat. Chem.* **2021**, *13*, 956–962.

[5] a) J. Steube, A. Kruse, O. S. Bokareva, T. Reuter, S. Demeshko, R. Schoch, M. A. Argüello Cordero, A. Krishna, S. Hohloch, F. Meyer, K. Heinze, O. Kühn, S. Lochbrunner, M. Bauer, *Nat. Chem.* **2023**, *15*, 468–474; b) W. Leis, M. A. Argüello Cordero, S. Lochbrunner, H. Schubert, A. Berkefeld, *J. Am. Chem. Soc.* **2022**, *144*, 1169–1173; c) K. S. Kjær, N. Kaul, O. Prakash, P. Chábera, N. W. Rosemann, A. Honarfar, O. Gordivska, L. A. Fredin, K.-E. Bergquist, L. Häggström, T. Ericsson, L. Lindh, A. Yartsev, S. Styring, P. Huang, J. Uhlig, J. Bendix, D. Strand, V. Sundström, P. Persson, R. Lomoth, K. Wärnmark, *Science* **2019**, *363*, 249–253.

[6] a) M. M. Alowakennu, A. Ghosh, J. K. McCusker, *J. Am. Chem. Soc.* **2023**, *145*, 20786–20791; b) N. Sinha, B. Pfund, C. Wegeberg, A. Prescimone, O. S. Wenger, *J. Am. Chem. Soc.* **2022**, *144*, 9859–9873; c) A. Y. Chan, A. Ghosh, J. T. Yarranton, J. Twilton, J. Jin, D. M. Arias-Rotondo, H. A. Sakai, J. K. McCusker, D. W. C. MacMillan, *Science* **2023**, *382*, 191–197.

[7] T. Ogawa, O. S. Wenger, *Angew. Chem. Int. Ed.* **2023**, *62*, e202312851.

[8] a) R. Hamze, J. L. Peltier, D. Sylvinson, M. Jung, J. Cardenas, R. Haiges, M. Soleilhavoup, R. Jazzar, P. I. Djurovich, G. Bertrand, M. E. Thompson, *Science* **2019**, *363*, 601–606; b) M. Gernert, L. Balles-Wolf, F. Kerner, U. Müller, A. Schmiedel, M. Holzapfel, C. M. Marian, J. Pflaum, C. Lambert, A. Steffen, *J. Am. Chem. Soc.* **2020**, *142*, 8897–8909; c) A. M. T. Muthig, O. Mrózek, T. Ferschke, M. Rödel, B. Ewald, J. Kuhnt, C. Lenczyk, J. Pflaum, A. Steffen, *J. Am. Chem. Soc.* **2023**, *145*, 4438–4449; d) A. M. T. Muthig, J. Wieland, S. Koop, C. Lenczyk, F. Kerner, B. Hupp, A. Steffen, *Inorg. Chem.* **2022**, *61*, 17427–17437; e) A. Hossain, A. Bhattacharyya, O. Reiser, *Science* **2019**, *364*, eaav9713; f) A. M. T. Muthig, M. Krumrein, J. Wieland, M. Gernert, F. Kerner, J. Pflaum, A. Steffen, *Inorg. Chem.* **2022**, *61*, 14833–14844; g) C. N. Muniz, J. Schaab, A. Razgoniaev, P. I. Djurovich, M. E. Thompson, *J. Am. Chem. Soc.* **2022**, *144*, 17916–17928; h) C. N. Muniz, C. A. Archer, J. S. Applebaum, A. Alagaratnam, J. Schaab, P. I. Djurovich, M. E. Thompson, *J. Am. Chem. Soc.* **2023**, *145*, 13846–13857.

[9] a) J. Nitsch, F. Lacemon, A. Lorbach, A. Eichhorn, F. Cisnetti, A. Steffen, *Chem. Commun.* **2016**, *52*, 2932–2935; b) B. Hupp, J. Nitsch, T. Schmitt, R. Bertermann, K. Edkins, F. Hirsch, I. Fischer, M. Auth, A. Sperlich, A. Steffen, *Angew. Chem. Int. Ed.* **2018**, *57*, 13671–13675; c) L. Bergmann, J. Friedrichs, M. Mydlak, T. Baumann, M. Nieger, S. Bräse, *Chem. Commun.* **2013**, *49*, 6501–6503.

[10] a) R. Hamze, S. Shi, S. C. Kapper, D. S. Muthiah Ravinson, L. Estergreen, M.-C. Jung, A. C. Tadle, R. Haiges, P. I. Djurovich, J. L. Peltier, R. Jazzar, G. Bertrand, S. E. Bradforth, M. E. Thompson, *J. Am. Chem. Soc.* **2019**, *141*, 8616–8626; b) H. Yersin, D. Donges, in *Transition Metal and Rare Earth Compounds: Excited States, Transitions, Interactions II* (Ed.: H. Yersin), Springer Berlin Heidelberg, Berlin, **2001**, pp. 81–186; c) A. M. T. Muthig, B. Ewald, T. H. Ferschke, J. Pflaum, A. Steffen, PCT/EP2022/073938, **2022**; d) J. Ma, J. Schaab, S. Paul, S. R. Forrest, P. I. Djurovich, M. E. Thompson, *J. Am. Chem. Soc.* **2023**, *145*, 20097–20108.

[11] a) I. B. Lozada, J. D. Braun, J. A. G. Williams, D. E. Herbert, *Inorg. Chem.* **2022**, *61*, 17568–17578; b) V. Ferraro, F. Baggio, J. Castro, M. Bortoluzzi, *Eur. J. Inorg. Chem.* **2022**, e202200119; c) D. Temerova, K. S. Kisel, T. Eskelinen, A. S. Melnikov, N. Kinnunen, P. Hirva, J. R. Shakirova, S. P. Tunik, E. V. Grachova, I. O. Koshevoy, *Inorg. Chem. Front.* **2021**, *8*, 2549–2560; d) Z. Mahmood, N. Rehmat, S. Ji, J. Zhao, S. Sun, M. Di Donato, M. Li, M. Teddei, Y. Huo, *Chem. Eur. J.* **2020**, *26*, 14912–14918; e) B. Goswami, T. J. Feuerstein, R. Yadav, S. Lebedkin, P. J. Boden, S. T. Steiger, G. Niedner-Schatteburg, M. Gerhards, M. M. Kappes, P. W. Roesky, *Chem. Eur. J.* **2021**, *27*, 15110–15119; f) J. Xiong, K. Li, T. Teng, X. Chang, Y. Wei, C. Wu, C. Yang, *Chem. Eur. J.* **2020**, *26*, 6887–6893; g) K. D. Oyler, F. J. Coughlin, S. Bernhard, *J. Am. Chem. Soc.*

2007, *129*, 210–217; h) R. G. Highland, G. A. Crosby, *Chem. Phys. Lett.* **1985**, *119*, 454–458; i) K. A. Truesdell, G. A. Crosby, *J. Am. Chem. Soc.* **1985**, *107*, 1787–1788; j) Y. Sakai, Y. Sagara, H. Nomura, N. Nakamura, Y. Suzuki, H. Miyazaki, C. Adachi, *Chem. Commun.* **2015**, *51*, 3181–3184.
[12] J. A. Kübler, B. Pfund, O. S. Wenger, *JACS Au* **2022**, *2*, 2367–2380.
[13] N. Lüdtke, J. Kuhnt, T. Heil, A. Steffen, C. M. Marian, *ChemPhotoChem* **2023**, *7*, e202200142.
[14] H. Noda, H. Nakanotani, C. Adachi, *Sci. Adv.* **2018**, *4*, eaao6910.
[15] a) O. Mrózek, M. Gernert, A. Belyaev, M. Mitra, L. Janiak, C. M. Marian, A. Steffen, *Chem. Eur. J.* **2022**, *28*, e202201114; b) O. Mrózek, M. Mitra, B. Hupp, A. Belyaev, N. Lüdtke, D. Wagner, C. Wang, O. S. Wenger, C. M. Marian, A. Steffen, *Chem. Eur. J.* **2023**, *29*, e202203980.
[16] V. Lavallo, Y. Canac, C. Präsang, B. Donnadieu, G. Bertrand, *Angew. Chem. Int. Ed.* **2005**, *44*, 5705–5709.
[17] Deposition numbers 2290921 (for **1**), 2290922 (for **CZT1**), 2290923 (for **CZT2**), 2290925 (for **CZT3a**) and 2290924 (for **CZT3b**) contain the supplementary crystallographic data for this paper. These data are provided free of charge by the joint Cambridge Crystallographic Data Centre and Fachinformationszentrum Karlsruhe Access Structures service.
[18] a) M. Tesmer, H. Vahrenkamp, *Eur. J. Inorg. Chem.* **2001**, 1183–1188; b) K. Halvorsen, G. A. Crosby, W. F. Wacholtz, *Inorg. Chim. Acta* **1995**, *228*, 81–88.
[19] A. Steinegger, S. M. Borisov, *ACS Omega* **2020**, *5*, 7729–7737.
[20] W. L. F. Armarego, *Purification of laboratory Chemicals*, Butterworth Heinemann, Oxford, **1996**.
[21] R. Jazzar, J. Bourg, R. D. Dewhurst, B. Donnadieu, G. Bertrand, *J. Org. Chem.* **2007**, *72*, 3492–3499.
[22] M. Deng, N. F. M. Mukhtar, N. D. Schley, G. Ung, *Angew. Chem. Int. Ed.* **2020**, *59*, 1228–1231.
[23] Gaussian 16, revision A.03, M. J. Frisch, G. W. Trucks, H. B. Schlegel, G. E. Scuseria, M. A. Robb, J. R. Cheeseman, G. Scalmani, V. Barone, G. A. Petersson, H. Nakatsuji, et al., Gaussian Inc.: Wallingford CT, **2016**.
[24] E. Cancès, B. Mennucc, J. Tomasi, *J. Chem. Phys.* **1997**, *107*, 3032–3041.
[25] B. Mennucci, E. Cancès, J. Tomasi, *J. Phys. Chem. B* **1997**, *101*, 10506–10517.
[26] C. Lee, W. Yang, R. G. Parr, *Phys. Rev. B* **1988**, *37*, 785–789.
[27] A. D. Becke, *J. Chem. Phys.* **1993**, *98*, 1372–1377.
[28] A. Schäfer, H. Horn, R. Ahlrichs, *J. Chem. Phys.* **1992**, *97*, 2571–2577.
[29] D. Figgen, G. Rauhut, M. Dolg, H. Stoll, *Data. Chem. Phys.* **2005**, *311*, 227–244.
[30] S. Grimme, M. Waletzke, *J. Chem. Phys.* **1999**, *111*, 5645–5655.
[31] C. M. Marian, A. Heil, M. Kleinschmidt, *Wiley Interdiscip. Rev.: Comput. Mol. Sci.* **2019**, *9*, e1394.
[32] A. Heil, M. Kleinschmidt, C. M. Marian, *J. Chem. Phys.* **2018**, *149*, 164106.
[33] R. Ahlrichs, M. Bär, M. Häser, H. Horn, C. Kölmel, *Chem. Phys. Lett.* **1989**, *162*, 165–169.
[34] TURBOMOLE V6.6 2014, a development of University of Karlsruhe and Forschungszentrum Karlsruhe GmbH, 1989–2007, TURBOMOLE GmbH, since 2007; available from http://www.turbomole.com.
[35] M. Kleinschmidt, J. Tatchen, C. M. Marian, *J. Comput. Chem.* **2002**, *23*, 824–833.
[36] M. Kleinschmidt, C. M. Marian, *Chem. Phys.* **2005**, *311*, 71–79.
[37] B. A. Heß, C. M. Marian, U. Wahlgren, O. Gropen, *Chem. Phys. Lett.* **1996**, *251*, 365–371.
[38] AMFI is an atomic spin-orbit integral program written by B. Schimmelpfennig, University of Stockholm, **1996**.
[39] M. Kleinschmidt, J. Tatchen, C. M. Marian, *J. Chem. Phys.* **2006**, *124*, 124101.
[40] M. Etinski, J. Tatchen, C. M. Marian *J. Chem. Phys.* **2011**, *134*, 154105.
[41] M. Etinski, J. Tatchen, C. M. Marian, *Phys. Chem. Chem. Phys.* **2014**, *16*, 4740–4751.
[42] P. S. Nejman, B. Morton-Fernandez, N. Black, D. B. Cordes, A. M. Slawin, P. Kilian, J. D. Woollins, *J. Organomet. Chem.* **2015**, *776*, 7–16.
[43] S. I. Etkind, J. Lopez, Y. G. Zhu, J. Fang, W. J. Ong, Y. Shao-Horn, T. M. Swager, *ACS Sustainable Chem. Eng.* **2022**, *10*, 11739–11750.
[44] G. M. Sheldrick, *Acta Crystallogr. Sect. C* **2015**, *71*, 3–8.
[45] G. M. Sheldrick, *Acta Crystallogr. Sect. A* **2015**, *71*, 3–8.
[46] O. V. Dolomanov, L. J. Bourhis, R. J. Gildea, J. A. K. Howard, H. Puschmann, *J. Appl. Crystallogr.* **2009**, *42*, 339–341.

Manuscript received: October 27, 2023
Accepted manuscript online: December 8, 2023
Version of record online: January 15, 2024